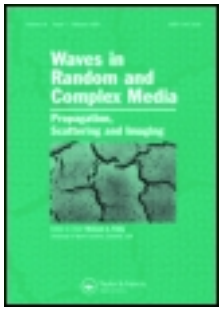

Waves in Random and Complex Media

Publication details, including instructions for authors and subscription information:
http://www.tandfonline.com/loi/twrm20

Negative refraction and dispersion phenomena in platonic clusters

Michael J.A. Smith [a] , Ross C. McPhedran [b] , Chris G. Poulton [c] & Michael H. Meylan [d]

[a] Department of Mathematics, The University of Auckland, Private Bag 92019, Auckland 1142, New Zealand

[b] CUDOS ARC Centre of Excellence, School of Physics, University of Sydney, New South Wales 2006, Sydney, Australia

[c] School of Mathematical Sciences, University of Technology, New South Wales 2007, Sydney, Australia

[d] School of Mathematical and Physical Sciences, The University of Newcastle, New South Wales 2308, Newcastle, Australia

Version of record first published: 02 Aug 2012

To cite this article: Michael J.A. Smith, Ross C. McPhedran, Chris G. Poulton & Michael H. Meylan (2012): Negative refraction and dispersion phenomena in platonic clusters, Waves in Random and Complex Media, DOI:10.1080/17455030.2012.711495

To link to this article: http://dx.doi.org/10.1080/17455030.2012.711495

Waves in Random and Complex Media
2012, 1–24, iFirst

Negative refraction and dispersion phenomena in platonic clusters

Michael J.A. Smith[a]*, Ross C. McPhedran[b], Chris G. Poulton[c] and Michael H. Meylan[d]

[a]*Department of Mathematics, The University of Auckland, Private Bag 92019, Auckland 1142, New Zealand;* [b]*CUDOS ARC Centre of Excellence, School of Physics, University of Sydney, New South Wales 2006, Sydney, Australia;* [c]*School of Mathematical Sciences, University of Technology, New South Wales 2007, Sydney, Australia;* [d]*School of Mathematical and Physical Sciences, The University of Newcastle, New South Wales 2308, Newcastle, Australia*

(*Received 16 April 2012; final version received 6 July 2012*)

We consider the problem of Gaussian beam scattering by finite arrays of pinned points, or platonic clusters, in a thin elastic plate governed by the biharmonic plate equation. Integral representations for Gaussian incident beams are constructed and numerically evaluated to demonstrate the different behaviours exhibited by these finite arrays. We show that it is possible to extend the scattering theory from infinite arrays of pinned points to these finite crystals, which exhibit the predicted behaviour well. Analytical expressions for the photonic superprism parameters p, q and r, which are measures for dispersion inside the crystal, are also derived for the pinned plate problem here. We demonstrate the existence of negative refraction, beam splitting, Rayleigh anomalies, internal reflection, and near-trapping on the first band surface, giving examples for each of these behaviours.

1. Introduction

The study of platonic crystals (PlaCs) is an emerging field and a sub-branch of the study of photonic crystals. A platonic crystal is, by analogy to a photonic crystal, a regular arrangement of scatterers where the propagation medium is governed by the biharmonic thin plate equation as opposed to the Helmholtz equation. While the problem of scattering in thin plates has a considerable history [1–3], the problem is quite challenging even for a single cavity, and in fact, the solution for an arbitrary shaped hole has only been found recently [4]. We are not interested here with complex scatterers but instead with the simplest scattering problem that can be imposed on a thin plate: scattering by regularly-spaced pins. This problem was first studied by Evans and Porter [5] and has recently been the subject of extensive work [6–10]. It turns out that this problem, while relatively simple to compute numerically, displays a wide range of complex behaviours, ranging from near trapping [8], to an analogue to electromagnetically induced transparency effects [9].

*Corresponding author. Email: m.smith@math.auckland.ac.nz

ISSN 1745–5030 print/ISSN 1745–5049 online

http://dx.doi.org/10.1080/17455030.2012.711495
http://www.tandfonline.com

While the problem of scattering by pins is mainly of theoretical interest, the thin plate has recently been the subject of experiments by Stenger *et al.* [11], who, motivated by Farhat *et al.* [3], demonstrated strong cloaking for a singular circular scatterer by elastodynamic waves in a wide frequency range. The importance of this experiment is discussed in the review article by McPhedran and Movchan [12]. More complicated platonic crystals, such as those containing defects, have also been examined by Poulton *et al.* [13] and Smith *et al.* [14]. One prominent feature of such crystals is the presence of modes which are highly localized within the defects.

For a PlaC comprised of pins (isotropic point scatterers), the linear system of equations can be formed and subsequently solved by direct inversion (with the exception of resonant frequencies, where the matrix is non-invertible [8]). This is a consequence of the fact that the Green's function for the biharmonic plate equation is regular as $kr \to 0$, in contrast to the Green's function for the Helmholtz equation, which is singular in the same limit. As such, the corresponding system for a cluster of pins under Helmholtz's equation requires a slight modification in order to be solved analytically – a procedure known as Foldy's method [15,16]. Other techniques, such as homogenization, could also be applied to compute the solution for such crystals, as shown by Krokhin *et al.* [17] for photonic crystals, and Poulton *et al.* [18] for periodic elastodynamic structures.

To understand the scattering behaviour of PlaCs a close examination of the band surfaces for the doubly periodic pinned problem is required. By using the band surfaces and the conservation condition at the interface one can obtain the group velocity vector direction, which determines the primary direction of the wave inside the periodic array of pins [19]. This method has been used to successfully predict the behaviour of water waves, photonic crystals and phononic crystals (e.g. [20–22]). However, this theory has never been applied to scattering in thin plates and we apply this approach for the first time here.

For a plate fixed at a doubly periodic set of points, an elegant dispersion relation is obtained in terms of elementary lattice sums, which was first shown by Movchan *et al.* [7], drawing upon an extensive body of research dedicated to the efficient evaluation of these sums in the context of photonic crystals, such as [6,23–26]. This dispersion relation reveals an infinite number of continuous band surfaces where propagation through the medium is supported. It is on the first band surface that we investigate the different scattering behaviours possible, including negative refraction. Band surfaces in photonic crystals have been used to explain several exotic refractive effects, including *negative refraction*, in which a wave is refracted at a photonic crystal interface by an angle with opposite sign to that of a homogeneous material. We discuss the conditions for negative refraction and associated dispersion phenomena for vibrations in thin plates for the first time here also.

In the context of constructing these slowness surfaces, the incident and refracted angles can exhibit extremely complex relations. For this reason Baba and Nakamura [27], Kosaka *et al.* [28], and Steel *et al.* [29] investigated the parameters p, q and r, which denote the generalized angular resolving power, generalized dispersion and resolution of the crystal respectively. These parameters examine the relationship between the frequency, incident angle and refraction angle of waves travelling through the structure, and thus act as measures of dispersion inside the crystal. We determine these parameters for our problem here and derive a new expression for q

and r in the platonic case. These parameters also help us identify where superprism or superlensing effects are possible in the platonic setting [21,30].

The refraction of waves by these crystals is extremely complicated and is not well illustrated if excited by plane long crested waves. We use here Gaussian incident beams of the form given by Elsherbeni *et al*. [31] and Marshall *et al*. [32] to clearly demonstrate the behaviour both inside and beyond the PlaC. These localized incident beams are constructed as a continuous superposition of travelling plane wave solutions to the Helmholtz equation. We demonstrate that the Gaussian beam can be efficiently evaluated by expanding it as a discrete superposition of plane waves using Gauss–Hermite quadrature. There is a large body of research dedicated to the construction of Gaussian wave packets in the time domain, as well as on the stability of Gaussian beams, and we direct the interested reader to [33–36].

We show that negative refraction is observed inside the PlaC, and is typically characterized by a negative Goos–Hanchen shift on the exit interface of the crystal, for non-shallow angles. Negative refraction effects have been previously observed in metamaterial slabs [37], thin plates with square cavities [3] and photonic crystals [38,39]. Here we also demonstrate that beam splitting [40] is possible for shallower angles of refraction. This is closely connected with the concept of shear wave splitting in seismology and geophysics [41], however we are unaware of any publications that identify beam splitting in a platonic context.

The outline of this paper is as follows. In Section 2 we introduce the solution to the problem of plane wave scattering by a finite PlaC. In Section 3 we outline how to construct Gaussian incident beams, and compute the response of the PlaC to these special incident waves. In Section 4 we consider the doubly periodic pin problem and compute the band surfaces to reveal information about the Bloch states of the crystal. In Section 5 we derive analytic expressions for the resolution parameters p, q and r which characterize both frequency and angular dispersion in platonic crystals. In Section 6 we show how to determine the angle of the reflected and transmitted beams. This is followed in Section 7 by a survey of the Brillouin zone, where a sample of behaviours is shown along with the p, q, r and effective index surfaces for the first band surface (which is also given). In Section 8 we provide a brief summary of the paper followed by Appendix 1 which outlines the numerical approach for computing the Gaussian beams discussed in Section 3.

2. Plane wave incidence

The governing equation for a thin elastic plate in two dimensions is given by the Euler–Bernoulli equation

$$\left(D\Delta^2 + \rho h \partial_t^2\right) u(\mathbf{x}; t) = 0, \tag{1a}$$

where u represents the out-of-plane displacement of the plate, Δ is the Laplacian and D, ρ and h represent the material properties of the plate [42]. Assuming the solution is time-harmonic $u(\mathbf{x}; t) = \mathrm{Re}\,\{w(\mathbf{x})\mathrm{e}^{-i\omega t}\}$ we can obtain the frequency domain form of the plate equation

$$(\Delta^2 - k^4)w(\mathbf{x}) = (\Delta + k^2)(\Delta - k^2)w(\mathbf{x}) = 0, \tag{1b}$$

where $k^2 = \omega\sqrt{\rho h/D}$ is the non-dimensionalized wave number and ω denotes the angular frequency. We first consider the problem of wave scattering when plane waves are incident upon a finite square geometry of pins, where at each pin location $\mathbf{x}_n$ we impose the condition

$$w(\mathbf{x}_n) = 0, \quad \text{for } n = 1, \ldots, N. \tag{2}$$

The solution method for scattering of a plane incident wave by a finite cluster of pins is well known [5,7] and can be applied to any finite arrangement of pins, including irregular and defective geometries. It is included here for completeness. The incident wave is taken to be of the form

$$w^i(\mathbf{x}) = \mathrm{e}^{\mathrm{i}(k_{0x}x - k_{0y}y)}, \tag{3}$$

where $k_{0x} = k\sin\theta_i$ and $k_{0y} = \sqrt{k^2 - k_{0x}^2} = k\cos\theta_i$. A schematic of the problem is given in Figure 1, showing the orientation of the incident and refracted wave angles. We can consider each of these pins as representing point sources of various strengths. This allows us to expand the solution as the incident wave plus a superposition of Green's functions centred about each pin:

$$w(\mathbf{x}) = w^i(\mathbf{x}) + \sum_{n=1}^{N} a_n g(|\mathbf{x} - \mathbf{x}_n|), \tag{4}$$

where a_n represents the amplitude corresponding to the nth pin. The Green's function $g(r)$ satisfies

$$(\Delta^2 - k^4)\, g(r) = \delta(r), \tag{5a}$$

and is given in closed form by

$$g(r) = \frac{\mathrm{i}}{8k^2}\left[H_0^{(1)}(kr) - \frac{2}{\pi\mathrm{i}}K_0(kr)\right], \tag{5b}$$

where $r = |\mathbf{x} - \mathbf{x}'|$, $H_0^{(1)}$ is a zero-order Hankel function of the first kind and K_0 is a modified Bessel function of order zero [23,24].

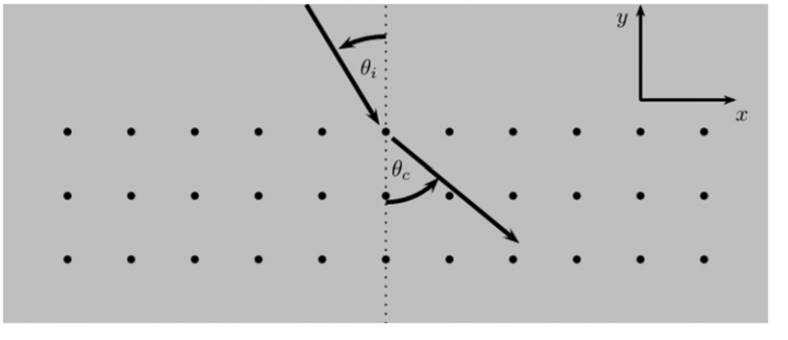

Figure 1. Infinite thin plate with a PlaC showing incident angle θ_i and angle of the group velocity θ_c for a localized incident wave.

To solve this problem, we apply the boundary condition (2) at each of these pinned points admitting

$$0 = w^i(\mathbf{x}_m) + \sum_{n=1}^{N} a_n g(|\mathbf{x}_m - \mathbf{x}_n|), \quad \text{for } m = 1, 2, \ldots, N, \tag{6}$$

which is an $N \times N$ linear system that can be solved directly to recover the unknown a_n amplitudes, and thus determine the displacement at any point in the domain. For the platonic problem here we observe that the Green's function is regular as r tends to zero ($g(0) = \mathrm{i}/8k^2$), in contrast to the Green's function for Helmholtz's equation which is unbounded.

Using this plane wave solution approach we can construct more complicated incident waves, including Gaussian beams. This is the topic of the following section.

3. Gaussian beam incidence

As outlined in [40,43], solutions to Helmholtz's equation

$$\left(\Delta + k^2\right) w(x, y) = 0,$$

can be expressed in the form

$$w(x, y) = \int_{-\infty}^{\infty} A(\alpha) \mathrm{e}^{\mathrm{i}\alpha x + \mathrm{i}\sqrt{k^2 - \alpha^2} y} \, \mathrm{d}\alpha, \tag{7a}$$

where

$$A(\alpha) = \frac{1}{2\pi} \int_{-\infty}^{\infty} w(x, 0) \mathrm{e}^{-\mathrm{i}\alpha x} \, \mathrm{d}x, \tag{7b}$$

and $w(x, 0)$ denotes an initial beam profile at $y = 0$. Here we consider a one-dimensional Gaussian initial profile given by

$$w(x, 0) = \exp(-x^2/W^2) \exp(\mathrm{i}k_{0x} x), \tag{8}$$

where $\exp(\mathrm{i}k_{0x}x)$ is the modulation envelope, and $2W$ is the full width at half maximum of the Gaussian (FWHM). Substituting this initial profile into expressions (7b) and (7a) we can obtain the Gaussian beam expression

$$w(x, y) = \frac{W}{2\sqrt{\pi}} \int_{-\infty}^{\infty} \mathrm{e}^{-(\alpha - k_{0x})^2 W^2/4} \mathrm{e}^{\mathrm{i}\alpha x + \mathrm{i}\sqrt{k^2 - \alpha^2} y} \, \mathrm{d}\alpha, \tag{9}$$

which represents a Gaussian beam travelling in the direction of $y > 0$ where the profile $w(x, 0)$ is perfectly reconstructed at $y = 0$. Observe that in (9) the Gaussian beam is expressed as a continuous weighted superposition of plane waves that have *a fixed wave number* k, but are considered over *multiple incident directions*, with the primary direction defined by the carrier wave value k_{0x}.

It is a straightforward extension from (9) to construct a Gaussian incident wave where the initial profile is refocussed at some point (x_0, y_0) above the cluster and

travelling in the direction $y < 0$. This expression is given by

$$w_G^i(x,y) = \frac{W}{2\sqrt{\pi}} \int_{-\infty}^{\infty} \mathrm{e}^{-(\alpha - k_{0x})^2 W^2/4} \, \mathrm{e}^{\mathrm{i}\alpha(x-x_0) - \mathrm{i}\sqrt{k^2-\alpha^2}(y-y_0)} \, \mathrm{d}\alpha, \tag{10}$$

and is analogous to the form given in [31,32]. Note that the Gaussian integral forms (10) and (9) have one strong disadvantage in that some of the component plane waves become evanescent at large angles of incidence (that is $k^2 - \alpha^2 < 0$) causing a reduction in the plane wave component of the beam (but ultimately not contributing to the total wave field in the far-field region). To overcome this issue completely we can instead consider a normally incident Gaussian beam and rotate our coordinate system by the desired incident angle, revealing

$$w_G^i(x,y) = \int_{-\infty}^{\infty} f(\alpha) \, \mathrm{e}^{\mathrm{i}\rho(\alpha)x - \mathrm{i}\sqrt{k^2-\rho(\alpha)^2}y} \, \mathrm{d}\alpha, \tag{11}$$

where $\rho(\alpha) = \alpha \cos\theta_i + \sqrt{k^2 - \alpha^2} \sin\theta_i$ and $f(\alpha) = W/(2\sqrt{\pi}) \exp\{-(\alpha W)^2/4\}$. Qualitatively, both of these expressions reveal identical scattering profiles, however the latter expression avoids the issue of component incident waves being evanescent completely and so we consider the final form (11) here.

Having constructed a Gaussian incident beam in the absence of a finite cluster we now need to include the scattering effects of our PlaC. Returning to Section 2 we recall that the scattered field for an incident plane wave is simply a sum of weighted Green's functions centred about all the pinned points. Thus, the total field for a Gaussian incident beam, including the response, can be represented as

$$w(x,y) = \int_{-\infty}^{\infty} f(\alpha) \left[w^i(\mathbf{x}) + \sum_{j=1}^{N} a_j g(|\mathbf{x} - \mathbf{x}_j|) \right] \mathrm{d}\alpha, \tag{12}$$

where $w^i(\mathbf{x}) = \exp\{\mathrm{i}\rho(\alpha)x - \mathrm{i}\sqrt{k^2 - \rho(\alpha)^2}y\}$ and $f(\alpha)$ represents the amplitude of each plane wave component.

One final consideration in constructing Gaussian beams is to determine the size of W. We can regard all of the Gaussian integral forms above as corresponding to an infinitely long screen containing a single aperture of width W with a source placed on one side. Providing that $W \geq \lambda$ then plane waves are able to pass through the aperture without interference, allowing the integral forms of the Gaussian to be constructed straightforwardly (which is a necessary condition for the representations given here). However if the width of the Gaussian W is small relative to the wavelength ($W < \lambda$) then circular waves emanate from the aperture creating difficulty in forming our required Gaussian. Finally, if W is large relative to the wavelength then plane waves emanate from the aperture, which can be easily shown by considering the definition of the Dirac delta function

$$\lim_{a \to 0} \frac{1}{a\sqrt{\pi}} \mathrm{e}^{-x^2/a^2} = \lim_{\xi \to \infty} \frac{\xi}{2\sqrt{\pi}} \mathrm{e}^{-x^2\xi^2/4} = \delta(x), \tag{13a}$$

which when substituted into (9) reveals

$$\lim_{W \to \infty} w = \int_{-\infty}^{\infty} \delta(\alpha - k_{0x}) \mathrm{e}^{\mathrm{i}\alpha x + \mathrm{i}\sqrt{k^2-\alpha^2}y} \, \mathrm{d}\alpha = \mathrm{e}^{\mathrm{i}k_{0x}x + \mathrm{i}\sqrt{k^2-k_{0x}^2}y}. \tag{13b}$$

We find that $W \simeq 2\lambda$ works well in general for the expressions above.

4. Wave propagation in infinite periodic arrays

We now consider the simple problem of zero forcing (no incident wave) in a doubly periodic infinite array of pins, which are arranged in a square lattice of period d. We represent the position of these pins by

$$\mathbf{R}_p = (nd, md), \quad p = (n, m), \quad m, n \in \mathbb{Z}, \tag{14}$$

and express the plate displacement as

$$w(x, y) = \sum_{m=-\infty}^{\infty} \sum_{n=-\infty}^{\infty} b_{mn}\, g(|\mathbf{x} - \mathbf{R}_p|), \tag{15}$$

where $g(r)$ is the Green's function given in (5b). Due to the perfect symmetry present in this problem, we need only consider computing the solution inside a fundamental cell around the origin known as the Wigner-Seitz cell [19]. Using the solution inside this primitive unit cell it is then possible to construct the solution throughout the entire plate via the quasi-periodicity condition

$$w(\mathbf{x} + \mathbf{R}_p) = w(\mathbf{x})\mathrm{e}^{\mathrm{i}\boldsymbol{\kappa}\cdot\mathbf{R}_p}, \tag{16}$$

where $\boldsymbol{\kappa} = (\kappa_x, \kappa_y)$ denotes the Bloch wave vector inside the crystal. Using this quasi-periodicity condition, (15) can be expressed in the form

$$w(x, y) = b_{00} \sum_{m=-\infty}^{\infty} \sum_{n=-\infty}^{\infty} \mathrm{e}^{\mathrm{i}\boldsymbol{\kappa}\cdot\mathbf{R}_p} g(|\mathbf{x} - \mathbf{R}_p|). \tag{17}$$

Since the quasi-periodicity has been built into the problem through the above condition, we need only apply the pin condition at the origin $u(0, 0) = 0$, revealing

$$\sum_p \mathrm{e}^{-\mathrm{i}\boldsymbol{\kappa}\cdot\mathbf{R}_p} g(|\mathbf{R}_p|) = 0, \tag{18}$$

after reversing the order of summation. The expression (18) can be simplified by use of Graf's addition theorem which is given by formula (9.1.79) in Abramowitz and Stegun [44] as

$$C_\nu(w)\mathrm{e}^{\mathrm{i}\nu\chi} = \sum_{l=-\infty}^{\infty} C_{l+\nu}(u) J_l(v)\mathrm{e}^{\mathrm{i}l\alpha}, \quad \text{where } |v\mathrm{e}^{\mathrm{i}\alpha}| < |u|, \tag{19}$$

where the lines u, v and w form a closed triangle with $w = \sqrt{u^2 + v^2 - 2uv\cos\alpha}$, α denoting the angle between the lines u and v, and χ denoting the angle between the lines u and w. Also, C_ν denotes a general Bessel function (J_ν, Y_ν, I_ν or K_ν). Applying the pin condition $u(\xi d, \eta d) = 0$ gives

$$\sum_p \mathrm{e}^{-\mathrm{i}\boldsymbol{\kappa}\cdot\mathbf{R}_p} g(|\mathbf{R}_{p'} - \mathbf{R}_p|) = 0, \tag{20}$$

where $\mathbf{R}_{p'} = (\xi \mathrm{d}, \eta d)$. Applying Graf's addition theorem to each Bessel function element of the Green's function in (20) reveals

$$H_0^{(1)}(k|\mathbf{R}_{p'} - \mathbf{R}_p|) = \sum_{l=-\infty}^{\infty} H_l^{(1)}(k|\mathbf{R}_p|) J_l(k|\mathbf{R}_{p'}|)\mathrm{e}^{\mathrm{i}l(\arg\mathbf{R}_p - \arg\mathbf{R}_{p'})}, \tag{21a}$$

$$K_0(k|\mathbf{R}_{p'} - \mathbf{R}_p|) = \sum_{l=-\infty}^{\infty} K_l(k|\mathbf{R}_p|) J_l(k|\mathbf{R}_{p'}|) \mathrm{e}^{\mathrm{i}l(\arg \mathbf{R}_p - \arg \mathbf{R}_{p'})}, \tag{21b}$$

which can only be applied when $|\mathbf{R}_p| > |\mathbf{R}_{p'}|$. Substituting these two representations into (20) then allows us to obtain

$$\left[H_0^{(1)}(k|\mathbf{R}_{p'}|) - \frac{2}{\pi \mathrm{i}} K_0(k|\mathbf{R}_{p'}|)\right] + \sum_{l=-\infty}^{\infty} \left\{S_l^H(k, \boldsymbol{\kappa}) - \frac{2}{\pi \mathrm{i}} S_l^K(k, \boldsymbol{\kappa})\right\} J_l(k|\mathbf{R}_{p'}|) \mathrm{e}^{-\mathrm{i}l \arg \mathbf{R}_{p'}} = 0, \tag{22}$$

where we know that $S_m^H(k, \boldsymbol{\kappa}) = -\delta_{m,0} + \mathrm{i} S_m^Y(k, \boldsymbol{\kappa})$,

$$S_m^Y(k, \boldsymbol{\kappa}) = \sum_{p \neq (0,0)} Y_m(k|\mathbf{R}_p|) \mathrm{e}^{\mathrm{i}m \arg \mathbf{R}_p} \mathrm{e}^{\mathrm{i}\boldsymbol{\kappa} \cdot \mathbf{R}_p}, \tag{23a}$$

$$S_m^K(k, \boldsymbol{\kappa}) = \sum_{p \neq (0,0)} K_m(k|\mathbf{R}_p|) \mathrm{e}^{\mathrm{i}m \arg \mathbf{R}_p} \mathrm{e}^{\mathrm{i}\boldsymbol{\kappa} \cdot \mathbf{R}_p}, \tag{23b}$$

from [6,25]. If we now designate $\xi = \eta = 0$, the final form of the dispersion relation can be obtained involving monopole terms alone:

$$S_0^Y(k, \boldsymbol{\kappa}) + \frac{2}{\pi} S_0^K(k, \boldsymbol{\kappa}) = 0. \tag{24}$$

The final difficulty that remains is that these lattice sums S_m^Y and S_m^K suffer from poor convergence. To remedy this issue, Movchan *et al.* [6] used the method of repeated integration to obtain convergent lattice sum expressions for the case of a square array

$$S_m^Y(k, \boldsymbol{\kappa}) = \frac{1}{J_{m+3}(k\xi)} \left(-\left[Y_3(k\xi) + \frac{1}{\pi} \sum_{n=1}^{3} \frac{(3-n)!}{(n-1)!} \left(\frac{2}{k\xi}\right)^{3-2n+2} \right] \delta_{m,0} \right.$$
$$\left. - \frac{4}{d^2} \mathrm{i}^m \sum_p \left(\frac{k}{Q_p}\right)^3 \frac{J_{m+3}(Q_p \xi)}{Q_p^2 - k^2} \mathrm{e}^{\mathrm{i}m\theta_p} \right), \tag{25a}$$

and

$$S_m^K(k, \boldsymbol{\kappa}) = \frac{1}{I_{m+3}(k\xi)} \left(\left[K_3(k\xi) - \frac{8}{(k\xi)^3} + \frac{1}{k\xi} - \frac{1}{8} k\xi \right] \delta_{m,0} + 2\pi \mathrm{i}^m \sum_p \left(\frac{k^3}{Q_p^3}\right) \frac{J_{m+3}(Q_p \xi) \mathrm{e}^{\mathrm{i}l\theta_p}}{Q_p^2 + k^2} \right), \tag{25b}$$

where δ_{mn} is the Kronecker delta, $\theta_p = \arg \mathbf{Q}_p$, $\mathbf{Q}_p = (\kappa_x + 2\pi n/d, \kappa_y + 2\pi m/d)$, $Q_p = \|\mathbf{Q}_p\|_2$, and the vector $\boldsymbol{\xi}$, with corresponding norm ξ, represents an arbitrary vector positioned inside the first Brillouin zone. Here we have used an acceleration parameter of 3, which is within the recommended range specified by Movchan *et al.* [6]. Care must be taken as numerical instability can be encountered when this parameter is unsuitably large [25].

An alternative expression to (24) can be obtained for our problem which is directly convergent and avoids the need to evaluate lattice sums completely. This is given in

[14]. It is from (24) that we are able to obtain band surfaces using the accelerated lattice sums defined above. That is, for a given Bloch vector $\boldsymbol{\kappa}$ the dispersion relation reveals values of k where propagation through the crystal is supported.

5. Platonic resolution parameters

Using the band surfaces, we know that it is a straightforward procedure to determine the direction of the group velocity inside a photonic crystal for a given incident angle and wave vector from inspection, assuming the crystal is suitably large [19]. However, the band diagram does not provide a full picture of how wave energy can behave *inside* a PlaC. To this end, Baba and Matsumoto [45] introduced three parameters: p, q, and r, to examine the degree of beam collimation, the degree of wavelength sensitivity, and the resolution of an incident beam inside a photonic crystal. We extend the theory from photonic crystals to our platonic problem here based on the theory outlined in [27,29,45] and we begin with the definitions

$$p = \left.\frac{\partial \theta_c}{\partial \theta_i}\right|_{\omega}, \tag{26a}$$

$$q = \left.\frac{\partial \theta_c}{\partial \omega}\right|_{\theta_i}, \tag{26b}$$

$$r = \frac{q}{p} = -\left.\frac{\partial \theta_i}{\partial \omega}\right|_{\theta_c}, \tag{26c}$$

where θ_c is the angle of refraction inside the crystal, as shown in Figure 1. To reiterate, p measures the sensitivity of θ_c to changes in input angle (for fixed frequency), q measures the change in refraction angle with respect to frequency (for fixed input angle), and r is defined as the resolution parameter, as in [45]. This theory was developed for the design of high resolution superprisms which are highly sensitive to both changes of input frequency and incident angle, in order steer the beam to desired angles. The theory outlined in this section is given in [29].

Here we examine PlaCs with flat entrance and exit interfaces only, and so there is a simplification of the model outlined. One of the core differences theoretically is that our dispersion relation is given by $\omega = k^2$ (that is, we specify $\sqrt{\rho h/D} = 1$ for all results here). This implies that outside the crystal $\omega = k_{0x}^2 + k_{0y}^2$, and inside the crystal $\omega = k^2$ for k values satisfying equation (24). The incident wave angle and refraction angle are defined as

$$\theta_c = \tan^{-1}\left(\frac{v_x}{v_y}\right), \quad \text{and} \quad \theta_i = \tan^{-1}\left(\frac{k_{0x}}{k_{0y}}\right), \tag{27}$$

where $\mathbf{v} = (v_x, v_y)$ represents the group velocity vector inside the crystal.

Returning to the definition of p in (26a) we can see that (after omitting the $|_{\omega}$ for ease of notation)

$$p = \frac{\partial \theta_c}{\partial \theta_i} = \frac{\partial}{\partial \theta_i}\tan^{-1}\left(\frac{v_x}{v_y}\right) = \frac{1}{|\mathbf{v}|^2}\left(v_y \frac{\partial v_x}{\partial \theta_i} - v_x \frac{\partial v_y}{\partial \theta_i}\right), \tag{28a}$$

which can be expressed in matrix form as

$$p = \frac{1}{|\mathbf{v}|^2}\left[\begin{array}{c|c} v_y & -v_x \end{array}\right]\left[\begin{array}{c} \partial v_x/\partial\theta_i \\ \hline \partial v_y/\partial\theta_i \end{array}\right]. \tag{28b}$$

In order to evaluate this expression we observe that the group velocity has the following dependence: $\mathbf{v} = \mathbf{v}(\boldsymbol{\kappa}\{\mathbf{k}_0(\theta_i, \omega)\})$, where $\boldsymbol{\kappa} = (\kappa_x, \kappa_y)$ is the PlaC wave vector and $\mathbf{k}_0 = (k_{0x}, k_{0y})$ is defined as the incident wave vector. After applying the chain rule we can represent these group velocity derivatives in matrix form directly from the definition of θ_c in (27), that is

$$\begin{bmatrix} \dfrac{\partial v_x}{\partial\theta_i} \\ \dfrac{\partial v_y}{\partial\theta_i} \end{bmatrix} = \begin{bmatrix} \dfrac{\partial^2\omega}{\partial\kappa_x\partial\kappa_x} & \dfrac{\partial^2\omega}{\partial\kappa_x\partial\kappa_y} \\ \dfrac{\partial^2\omega}{\partial\kappa_y\partial\kappa_x} & \dfrac{\partial^2\omega}{\partial\kappa_y\partial\kappa_y} \end{bmatrix} \begin{bmatrix} \dfrac{\partial\kappa_x}{\partial k_{0x}} & \dfrac{\partial\kappa_x}{\partial k_{0y}} \\ \dfrac{\partial\kappa_y}{\partial k_{0x}} & \dfrac{\partial\kappa_y}{\partial k_{0y}} \end{bmatrix} \begin{bmatrix} c\dfrac{\partial k_{0x}}{\partial\theta_i} \\ \dfrac{\partial k_{0y}}{\partial\theta_i} \end{bmatrix}, \tag{29a}$$

where

$$\begin{bmatrix} \dfrac{\partial\kappa_x}{\partial k_{0x}} & \dfrac{\partial\kappa_x}{\partial k_{0y}} \\ \dfrac{\partial\kappa_y}{\partial k_{0x}} & \dfrac{\partial\kappa_y}{\partial k_{0y}} \end{bmatrix} = \begin{bmatrix} \dfrac{\partial k_{0x}}{\partial\kappa_x} & \dfrac{\partial k_{0x}}{\partial\kappa_y} \\ \dfrac{\partial k_{0y}}{\partial\kappa_x} & \dfrac{\partial k_{0y}}{\partial\kappa_y} \end{bmatrix}^{-1}, \tag{29b}$$

by virtue of the inverse function theorem. To construct the second matrix of (29b) we make use of the conservation requirement that the tangential component of the incident and PlaC wave vectors must match at the interface, i.e. $k_{0x} = \kappa_x$ (which is a requirement in order for wave energy to be admitted into the crystal). Therefore $\partial k_{0x}/\partial\kappa_x = 1$ and $\partial k_{0x}/\partial\kappa_y = 0$. We also apply the $\partial/\partial\kappa_x$ and $\partial/\partial\kappa_y$ operators to the dispersion relation for the plate outside the crystal to reveal

$$\frac{\partial k_{0y}}{\partial\kappa_x} = \frac{1}{2k_{0y}}\left(\frac{\partial\omega}{\partial\kappa_x} - 2k_{0x}\right) \quad \text{and} \quad \frac{\partial k_{0x}}{\partial\kappa_x} = \frac{1}{2k_{0y}}\frac{\partial\omega}{\partial\kappa_y}, \tag{30}$$

thus allowing us to construct the first unknown matrix

$$\begin{bmatrix} \dfrac{\partial\kappa_x}{\partial k_{0x}} & \dfrac{\partial\kappa_x}{\partial k_{0y}} \\ \dfrac{\partial\kappa_y}{\partial k_{0x}} & \dfrac{\partial\kappa_y}{\partial k_{0y}} \end{bmatrix} = \left[\begin{array}{c|c} 1 & 0 \\ \hline \dfrac{1}{2k_{0y}}\left(\dfrac{\partial\omega}{\partial\kappa_x} - 2k_{0x}\right) & \dfrac{1}{2k_{0y}}\dfrac{\partial\omega}{\partial\kappa_y} \end{array}\right]^{-1} = \left[\begin{array}{c|c} 1 & 0 \\ \hline \dfrac{2k_{0x} - \partial\omega/\partial\kappa_x}{\partial\omega/\partial\kappa_y} & \dfrac{2k_{0y}}{\partial\omega/\partial\kappa_y} \end{array}\right]. \tag{31a}$$

To determine the final unknown vector in (29a) we can make use of the inverse function theorem once more and construct a Jacobian matrix involving derivatives of the incident wave vector $\mathbf{k}_0$ with respect to θ_i and ω:

$$\begin{bmatrix} \dfrac{\partial k_{0x}}{\partial\theta_i} & \dfrac{\partial k_{0x}}{\partial\omega} \\ \dfrac{\partial k_{0y}}{\partial\theta_i} & \dfrac{\partial k_{0y}}{\partial\omega} \end{bmatrix} = \begin{bmatrix} \dfrac{\partial\theta_i}{\partial k_{0x}} & \dfrac{\partial\theta_i}{\partial k_{0y}} \\ \dfrac{\partial\omega}{\partial k_{0x}} & \dfrac{\partial\omega}{\partial k_{0y}} \end{bmatrix}^{-1}. \tag{31b}$$

Note that our desired vector is given by the first column of (31b). We can differentiate the dispersion relation for the plate outside the crystal directly to reveal $\partial\omega/\partial k_{0x} = 2k_{0x}$ and $\partial\omega/\partial k_{0y} = 2k_{0y}$, and from the definition of θ_i in (27) we can compute the remaining elements

$$\frac{\partial\theta_i}{\partial k_{0x}} = \frac{k_{0y}}{\omega} \quad \text{and} \quad \frac{\partial\theta_i}{\partial k_{0y}} = -\frac{k_{0x}}{\omega}, \tag{32}$$

ultimately revealing

$$\begin{bmatrix} \dfrac{\partial k_{0x}}{\partial\theta_i} & \dfrac{\partial k_{0x}}{\partial\omega} \\ \dfrac{\partial k_{0y}}{\partial\theta_i} & \dfrac{\partial k_{0y}}{\partial\omega} \end{bmatrix} = \left[\begin{array}{c|c} \dfrac{k_{0y}}{\omega} & -\dfrac{k_{0x}}{\omega} \\ \hline 2k_{0x} & 2k_{0y} \end{array}\right]^{-1} = \left[\begin{array}{c|c} k_{0y} & \dfrac{k_{0x}}{2\omega} \\ \hline -k_{0x} & \dfrac{k_{0y}}{2\omega} \end{array}\right]. \tag{33}$$

After substituting the matrix (31a) and the first column of (33) into (29a) it is possible to determine the platonic form of p given in (28b). Expanding this admits the expression

$$\begin{aligned} p &= \frac{1}{|\mathbf{v}|^2}\left[\begin{array}{c|c} \dfrac{\partial\omega}{\partial\kappa_y} & -\dfrac{\partial\omega}{\partial\kappa_x} \end{array}\right]\left[\begin{array}{c|c} \dfrac{\partial^2\omega}{\partial\kappa_x\partial\kappa_x} & \dfrac{\partial^2\omega}{\partial\kappa_x\partial\kappa_y} \\ \hline \dfrac{\partial^2\omega}{\partial\kappa_y\partial\kappa_x} & \dfrac{\partial^2\omega}{\partial\kappa_y\partial\kappa_y} \end{array}\right]\left[\begin{array}{c|c} 1 & 0 \\ \hline \dfrac{2k_{0x} - \partial\omega/\partial\kappa_x}{\partial\omega/\partial\kappa_y} & \dfrac{2k_{0y}}{\partial\omega/\partial\kappa_y} \end{array}\right]\left[\begin{array}{c} k_{0y} \\ \hline -k_{0x} \end{array}\right] \\ &= \frac{1}{|\mathbf{v}|^2}\frac{k_{0y}}{\partial\omega/\partial\kappa_y}\left(\frac{\partial^2\omega}{\partial\kappa_x\partial\kappa_x}\left(\frac{\partial\omega}{\partial\kappa_y}\right)^2 + \frac{\partial^2\omega}{\partial\kappa_y\partial\kappa_y}\left(\frac{\partial\omega}{\partial\kappa_x}\right)^2 - 2\frac{\partial^2\omega}{\partial\kappa_x\partial\kappa_y}\frac{\partial\omega}{\partial\kappa_x}\frac{\partial\omega}{\partial\kappa_y}\right), \end{aligned} \tag{34}$$

which is identical to the photonic case, as given in [29]. Here we make use of the alternative representation for the group velocity $\mathbf{v} = (\partial\omega/\partial\kappa_x, \partial\omega/\partial\kappa_y)$.

For the purposes of calculating q we return to the original definition given in (26b) (after omitting the $|_{\theta_i}$ for ease of notation) to obtain

$$q = \frac{\partial\theta_c}{\partial\omega} = \frac{\partial}{\partial\omega}\tan^{-1}\left(\frac{v_x}{v_y}\right) = \frac{1}{|\mathbf{v}|^2}\left[\begin{array}{c|c} v_y & -v_x \end{array}\right]\left[\begin{array}{c} \partial v_x/\partial\omega \\ \hline \partial v_y/\partial\omega \end{array}\right]. \tag{35}$$

As before, we acknowledge the group velocity dependence $\mathbf{v} = \mathbf{v}\ (\boldsymbol{\kappa}\{\mathbf{k}_0(\theta_i, \omega)\})$ admitting

$$\begin{bmatrix} \dfrac{\partial v_x}{\partial\omega} \\ \dfrac{\partial v_y}{\partial\omega} \end{bmatrix} = \begin{bmatrix} \dfrac{\partial^2\omega}{\partial\kappa_x\partial\kappa_x} & \dfrac{\partial^2\omega}{\partial\kappa_x\partial\kappa_y} \\ \dfrac{\partial^2\omega}{\partial\kappa_y\partial\kappa_x} & \dfrac{\partial^2\omega}{\partial\kappa_y\partial\kappa_y} \end{bmatrix}\begin{bmatrix} \dfrac{\partial\kappa_x}{\partial k_{0x}} & \dfrac{\partial\kappa_x}{\partial k_{0y}} \\ \dfrac{\partial\kappa_y}{\partial k_{0x}} & \dfrac{\partial\kappa_y}{\partial k_{0y}} \end{bmatrix}\begin{bmatrix} \dfrac{\partial k_{0x}}{\partial\omega} \\ \dfrac{\partial k_{0y}}{\partial\omega} \end{bmatrix}, \tag{36}$$

where the second matrix is given by (31a) and the final vector is given by the second column of (33). The resulting substitutions allow us to obtain the

generalized dispersion

$$q = \frac{1}{|\mathbf{v}|^2}\begin{bmatrix} \dfrac{\partial\omega}{\partial\kappa_y} & \vdots & -\dfrac{\partial\omega}{\partial\kappa_x} \end{bmatrix}\begin{bmatrix} \dfrac{\partial^2\omega}{\partial\kappa_x\partial\kappa_x} & \vdots & \dfrac{\partial^2\omega}{\partial\kappa_x\partial\kappa_y} \\ \cdots & \vdots & \cdots \\ \dfrac{\partial^2\omega}{\partial\kappa_y\partial\kappa_x} & \vdots & \dfrac{\partial^2\omega}{\partial\kappa_y\partial\kappa_y} \end{bmatrix}\begin{bmatrix} 1 & \vdots & 0 \\ \cdots & \vdots & \cdots \\ \dfrac{2k_{0x} - \partial\omega/\partial\kappa_x}{\partial\omega/\partial\kappa_y} & \vdots & \dfrac{2k_{0y}}{\partial\omega/\partial\kappa_y} \end{bmatrix}\begin{bmatrix} \dfrac{\partial k_{0x}}{\partial\omega} \\ \cdots \\ \dfrac{\partial k_{0y}}{\partial\omega} \end{bmatrix},$$

$$= \frac{k_{0x}p}{2k_{0y}\omega} + \frac{1}{|\mathbf{v}|^2}\frac{1}{\partial\omega/\partial\kappa_y}\left(\frac{\partial^2\omega}{\partial\kappa_x\partial\kappa_y}\frac{\partial\omega}{\partial\kappa_y} - \frac{\partial^2\omega}{\partial\kappa_y^2}\frac{\partial\omega}{\partial\kappa_x}\right), \tag{37}$$

which is slightly different from the photonic q expression in [29] due to a 1/2 scaling factor in the first term. This arises from the fact that the dispersion relation for a PlaC is of the form $\omega = k^2$ as opposed to $\omega = k$ for photonic crystals. From the definition of p and q outlined above, it is a straightforward task to directly evaluate the platonic resolution expression

$$r = \frac{1}{k_{0y}}\left(\frac{k_{0x}}{2\omega} + \frac{k_{0y}}{|\mathbf{v}|^2 p}\frac{\partial^2\omega/\partial\kappa_x\partial\kappa_y\ \partial\omega/\partial\kappa_y - \partial^2\omega/\partial\kappa_y^2\ \partial\omega/\partial\kappa_x}{\partial\omega/\partial\kappa_y}\right), \tag{38}$$

which also differs by a 1/2 scaling factor in the first term compared to the photonic case.

6. Outside the crystal

It is a well known fact that the tangential component of the incident wave vector is always conserved when entering any number of different media in the plate [19] (i.e. here $\kappa_x = k_{0x}$). One direct consequence of this is that the grating equation completely determines all reflected and transmitted output angles above and below the crystal, regardless of crystal depth and group velocity.

The problem of computing output angles using the grating equation is a straightforward task; the angles are determined by

$$k_{px} = k\sin\theta_p = k_{0x} + 2\pi p/d \tag{39}$$

where $p \in \mathbb{Z}$ [40]. We can determine which orders are propagating and which are evanescent by computing

$$\chi_p = \begin{cases} \sqrt{k^2 - k_{px}^2} & \text{if } |k_{px}| \le k, \\ \mathrm{i}\sqrt{k_{px}^2 - k^2} & \text{if } |k_{px}| > k, \end{cases} \tag{40}$$

where real values of χ_p are associated with propagating orders. Consequently from (39) we can determine the required θ_p angles which exit the crystal from below at $(x_{out}, y_{out}) = (-dc_d\tan\theta_c, -dc_d)$, where c_d is the depth of the crystal.

7. Results and discussion

We construct the Gaussian beam outlined in the first section of this paper and consider a beam half-width $W = 5$. The following images are constructed using a cluster of 61 pins across (−30 to 30) and 11 gratings deep (0 to −10) in total.

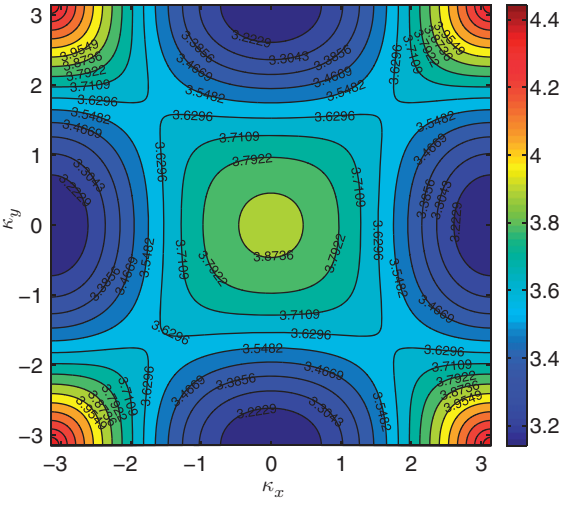

Figure 2. (Color online) Isofrequency contours for the first band surface over the first Brillouin zone.

This simple system exhibits very complex behaviour, and our aim here is to illustrate some interesting features of the first band surface, and is by no means exhaustive.

We begin by computing the equal value contours of k for the first band surface[1] from (24) (Figure 2). We observe a relative maximum at $(\kappa_x, \kappa_y) = (0, 0)$, absolute maxima at $(\pm\pi, \pm\pi)$, absolute minima at $(0, \pm\pi)$ and $(\pm\pi, 0)$, and saddle points at $(\pm 1.6650, \pm 1.6650)$. The first band occupies the interval $\pi < k < 4.4434$, below which a complete stop band exists, where no propagation through the crystal is possible at all. The first band surface for the pinned plate problem exhibits a much more complicated behaviour compared to the band surfaces seen in Steel *et al.* [29] for a photonic crystal of small-radius air holes in silicon, and Farhat *et al.* [3] for an array of square holes in a thin plate. Returning to Section 3, we recall that any incident Gaussian beams must satisfy $W \geq 2\pi/k$ and therefore a minimum waist of $W \geq 2$ must be considered for scattering on the first band surface.

Figure 3 shows the p, q and r contour plots for the platonic problem, where we follow the convention in Steel *et al.* [29] and plot $\log_{10}|1/p|$, $\log_{10}|q|$ and $\log_{10}|r|$, as $\log_{10}|r|$ is the sum of these other two quantities by definition. These contours are quite different from the photonic case shown in [29] due largely to the very different isofrequency contours in the platonic case, which exhibit a stronger degree of curvature comparatively. For our Gaussian beam scattering problem, which involves multiple incident directions θ_i, at a fixed frequency k, the most useful parameter here is p. Had we constructed a Gaussian beam in the time domain, which involves a superposition of plane waves of different wave numbers, then q (and subsequently r) would become a parameter of greater interest. Incidentally, we have been able to replicate these surfaces from the first principles definitions of these parameters, which gives us strong confidence in these results.

The final image 3(d) is the effective refractive index of the crystal, which follows directly from Snell's law $n_1/n_2 = \sin(\theta_c)/\sin(\theta_i)$, where $n_{1,2}$ denotes the refractive index of the first and second media respectively. This parameter n_1/n_2 also gives the ratio of

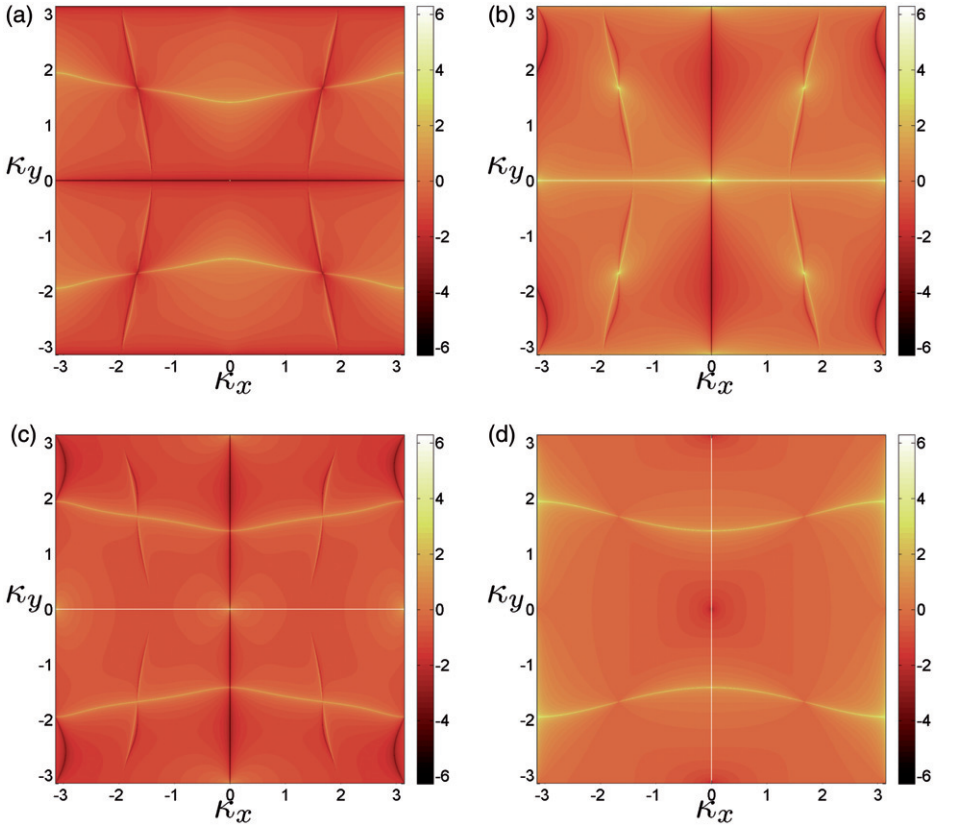

Figure 3. (Color online) (a) Surface plot of $\log_{10}|1 / p|$, (b) $\log_{10}|q|$, (c) $\log_{10}|r|$ and (d) $\log_{10}|n_1 / n_2|$ over the entire Brillouin zone.

the phase velocities inside the PlaC, allowing us to determine the speed with which the energy is transmitted through the crystal (Born and Wolf [40]).

On all of these plots we see standard and predictable behaviour in the form of smooth surfaces, with the exception of fine lines corresponding to extreme values which dissect the Brillouin zone, in part due to the curvature of the band surface. Notably, we see four interwoven vertical arcs in all of these surfaces that correspond to extremely high and extremely low parameter values, which intersect at the saddle points on the first band surface. Gaussian beams sent in at frequencies and angles which sit in the vicinity of this weaved structure are associated with near-trapped waves in the crystal which are highly leaky.

In Figure 3(a) we have two light parabolic arcs corresponding to small $|p|$, a line of high $|p|$ at $\kappa_y = 0$, and our four interwoven arcs of high and low $|p|$ which subtend the two parabolic arcs at the saddle points. These light parabolic arcs correspond to locations on the first band surface where the strongest vertical collimation is observed (and where the PlaC is least sensitive to changes in incident angle). The line at $\kappa_y = 0$ is where the surface is most sensitive to changes in incident angle. This line of high $|p|$ theoretically reveals where superlensing is possible (a superlens is a

photonic crystal where θ_c varies rapidly with changes in θ_i as discussed by Farhat *et al*. [3], and in a different context by Pendry and Smith [30]).

In Figure 3(b) we have a vertical line of low sensitivity to changes in wavelength at $\kappa_x = 0$ and a horizontal line of high sensitivity along $\kappa_y = 0$. We also have small corner parabolas of low sensitivity in all four corners of the Brillouin zone in addition to our four interwoven arcs seen previously in the $\log_{10}|1/p|$ figure.

In Figure 3(c) we observe all of the features seen in the two preceding figures, except that the line $\kappa_y = 0$ is now undefined as it corresponds to $q = 0$.

The final figure 3(d) is a surface of $\log_{10}|n_1/n_2|$, which shows that the speed of the wavefronts inside the crystal is at its lowest along the two horizontal parabolic arcs seen in Figure 3(a), reaching a minimum near the origin. There is a vertical line of infinite effective index corresponding to where θ_c is zero. Such very high values of refractive index correspond to what is termed ultra-refraction in the photonic crystal literature [46]. Using this surface one could easily determine thin segments on the first band surface where the effective index is $n_1/n_2 = -1$, and thus obtain the perfect lens discussed by Pendry [21], however due to the finiteness of the PlaC this may be difficult to observe and is not examined here.

We now move onto examining some examples of the different behaviours seen inside the first band surface in Figures 4–10. For a number of the examples given (such as Figure 4(a)) we provide corresponding slowness contours, which are figures of the band surface contours at a desired k value, superposed with the interface conservation condition k_{0x} given by the broken red line, and a blue circle which represents all possible incident wave directions at our fixed k. An associated incident wave vector is shown at the desired θ_i angle, and the edge of the first Brillouin zone is outlined by a grey box. The origin of the group velocity vector is given by the intersection of the broken red line with the solid black contour cuts (because of the periodicity there are usually only two cuts, and we choose the cut which physically corresponds to the direction where energy is admitted into the crystal). The direction of the group velocity vector is given by the normal of the isofrequency contour at this intersection point, pointing in the direction of increasing k.

Also shown are pictures of the displacement $\mathrm{Re}(u)$ inside the PlaC, and a picture of the crystal and the surrounding plate region (such as Figure 4(b) and (c)). For the larger picture, the incident ray vectors and associated crystal vectors are superposed on top of the field unless they extend well beyond the x limits of the figure. Note that as these are pictures of the displacement in the frequency domain, we view each of these field images as (usually) different snapshots in time of the time-harmonic displacement field.

We begin in Figure 4 with an example of negative refraction. In particular, Figure 4(a) is the slowness contour which clearly shows the direction of the group velocity at our chosen input parameters (given by the magenta arrow). At this particular k we also see the location of partial stop bands, which corresponds to where the vertical k_{0x} line would not intersect with a band surface contour. Figure 4(b) provides a close-up of the plate displacement inside the crystal, which clearly shows the wavefronts rotated at a negative angle relative to the incident beam angle. However, we note here that the angle of these phase fronts does not always correspond to the direction of wave energy propagation, which is always given by the group velocity angle. That is, the phase velocity and group velocity are usually quite disconnected inside the crystal, which demonstrates the highly anisotropic nature

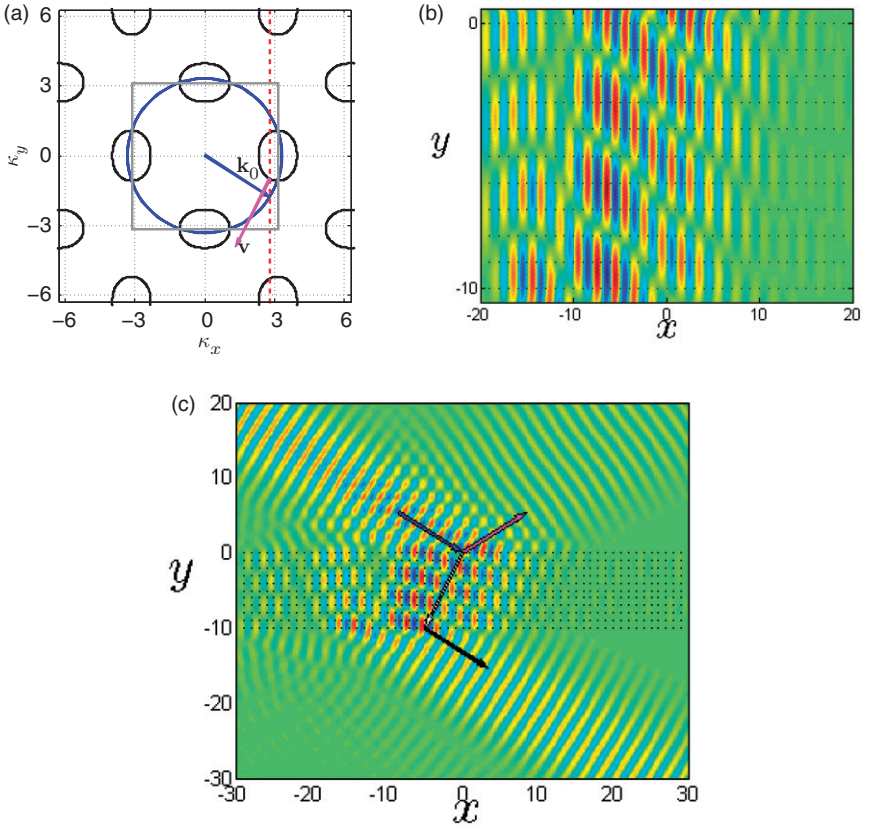

Figure 4. (Color online) (a): Slowness contour, and (b), (c): displacement (Re(u)) of the plate (where $k = 3\ .\ 3194$, $k_{0x} = 2.8084$, $\theta_i = 57.78^\circ$) demonstrating negative refraction.

of PlaCs. This is reinforced in Figure 4(c) where the arrow within the platonic crystal structure indicates the direction of the group velocity, which we note does not coincide with the phase front direction.

Inside the finite grating stack we can see some leakage horizontally along the cluster along the direction of periodicity. This small variation in the behaviour is entirely to be expected given that we are applying infinite theory to PlaCs of finite size, and thus that we are not able to achieve perfectly regular behaviour within the crystal. Regardless of this, the theory is still able to work well in achieving the desired behaviour, as demonstrated by Figure 4(c). Here we see the Gaussian beam striking the cluster from above, with a weaker beam reflected above the cluster. We also see a strong transmitted beam which has undergone a negative Goos–Hanchen shift on the exit interface of the crystal, giving us confirmation that negative refraction has actually taken place inside the crystal [40]. The reflected and transmitted beams may take some time to resolve to their predicted angles, given the local evanescent behaviour of the PlaC.

In Figure 5 we provide a typical example of platonic beam splitting, which is observed in a large section of the first band surface. Beam splitting is associated with

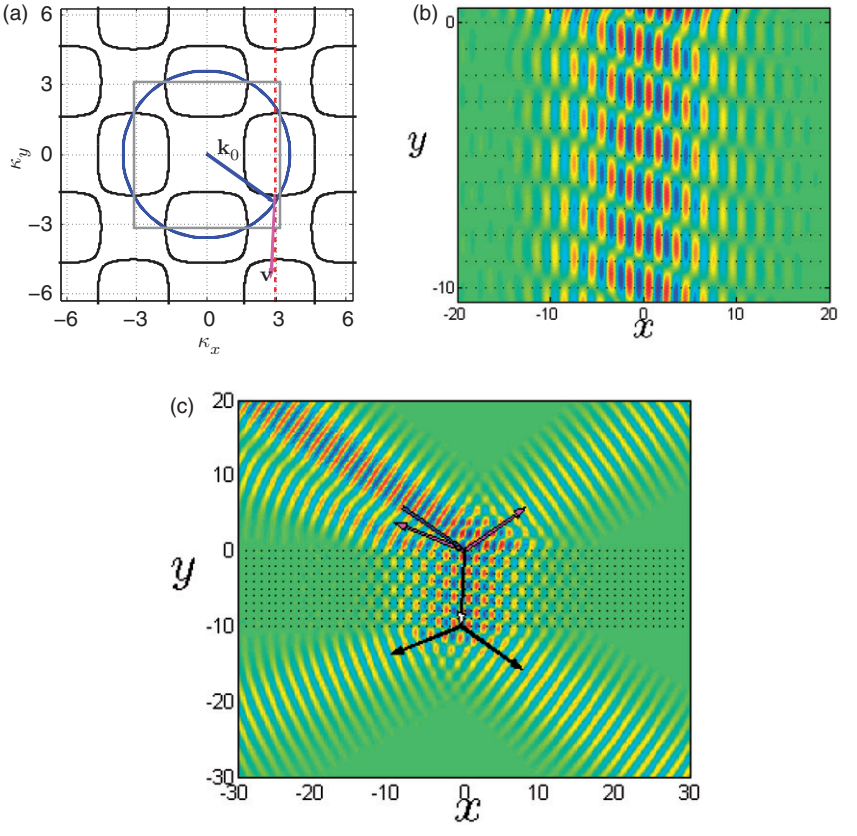

Figure 5. (Color online) (a): Slowness contour, and (b), (c): displacement (Re(u)) of the plate (where $k = 3.6022$, $k_{0x} = 2.95$, $\theta_i = 54.98^\circ$) demonstrating beam splitting.

both high $|p|$ and effective index values as there is strong vertical collimation, $\theta_c \simeq 0$, implying that the phase velocity inside the crystal is slow compared to the incident beam. The slowness contour in Figure 5(a) predicts a very shallow angle of refraction inside the crystal, which is confirmed in the subsequent images of the displacement. Figure 5(b) also shows that the phase fronts inside are highly rotated relative to the group velocity angle, and Figure 5(c) shows the excitation of two beams above and below the PlaC. Notably, above the cluster the excited beam interacts with the incident Gaussian creating a clear trough of minimal displacement.

Since the angle of refraction for beam splitting is often negative, it technically doubles as an example of negative refraction, however, no negative Goos–Hanchen shift is clearly observable and in its place we have two output beams, which can be explained by (39) above as two orders are excited ($\chi_{0,-1} \in \mathbb{R}$) under such a configuration.

To demonstrate that perfect vertical collimation is possible under this setting we provide an example of Littrow splitting in Figure 6. This is a platonic analogue to the Littrow configuration seen in optics [40], where the grating orders are excited in such a way that the incident beam is reflected back from the direction at which it came

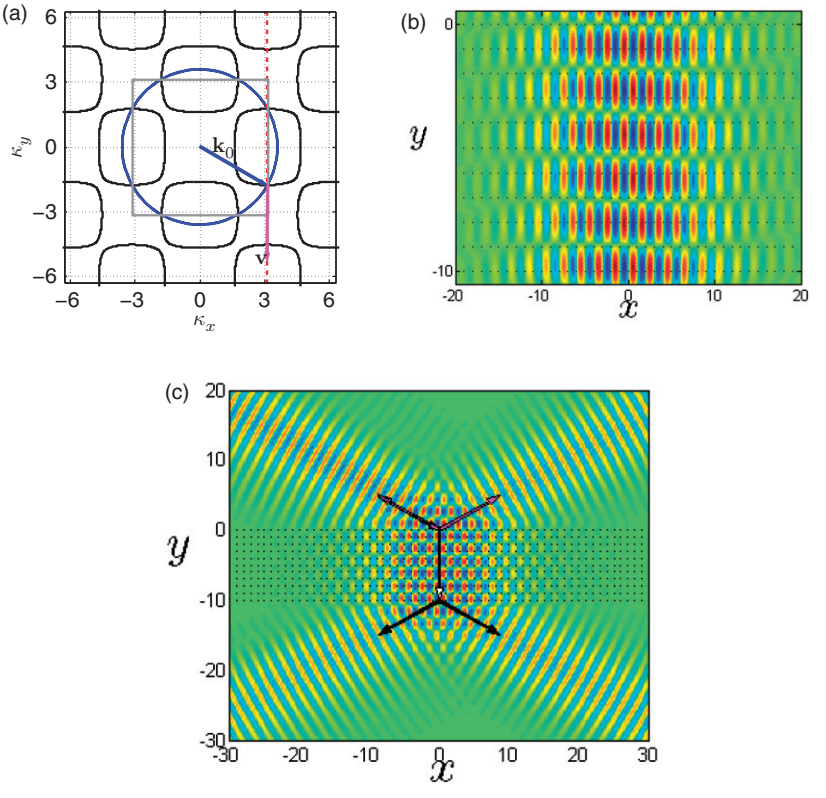

Figure 6. (Color online) (a): Slowness contour, and (b), (c): displacement (Re(u)) of the plate (where $k = 3.6022$, $k_{0x} = \pi$, $\theta_i = 60.71^\circ$) demonstrating Littrow beam splitting.

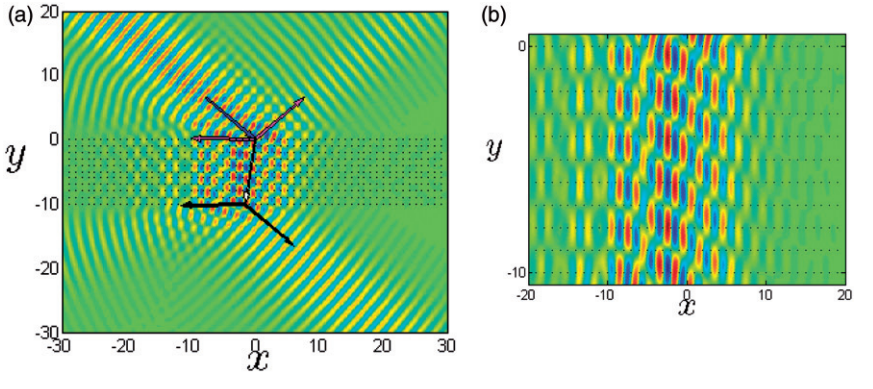

Figure 7. (Color online) (a), (b): Displacement (Re(u)) of the plate (where $k = 3.5697$, $k_{0x} = 2.7174$, $\theta_i = 49.57^\circ$) demonstrating a Rayleigh anomaly.

(i.e. retroreflected), creating a perfectly symmetric field. We can determine when this takes place by setting $\theta_i = -\theta_p$ in (39) to obtain the Littrow condition

$$2k\sin(\theta_i) = 2\pi p/d.$$

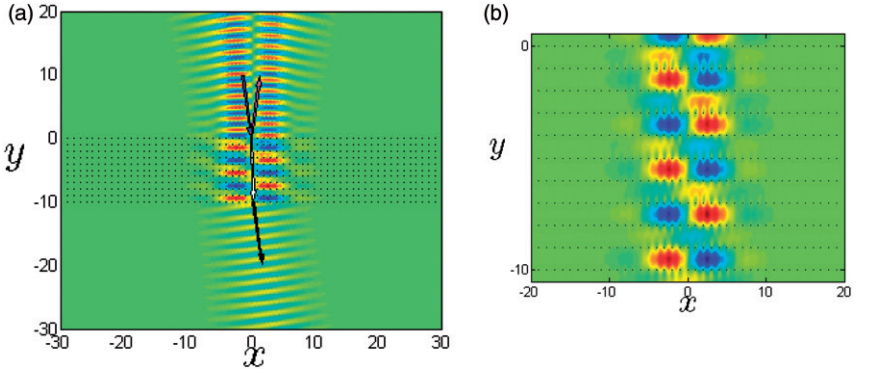

Figure 8. (Color online) (a), (b): Displacement (Re(u)) of the plate (where $k = 3.6373$, $k_{0x} = 0.50$, $\theta_i = 7.90^\circ$) demonstrating internal reflection.

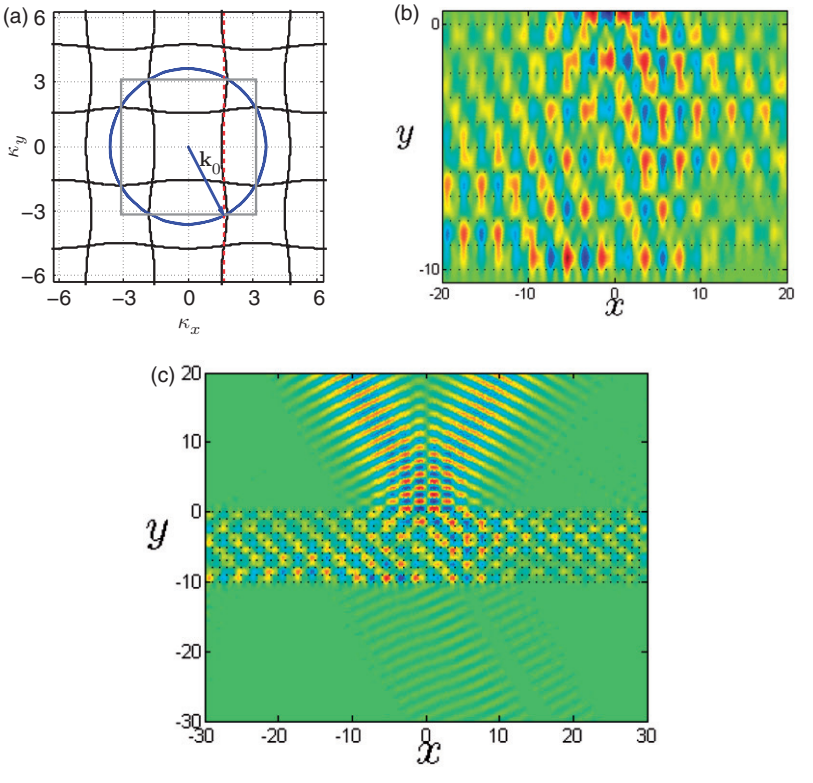

Figure 9. (Color online) (a): Slowness contour, and (b), (c): displacement (Re(u)) of the plate (where $k = 3.6239$, $k_{0x} = 1.665$, $\theta_i = 27.35^\circ$) demonstrating behaviour at the saddle point (near trapped waves).

Compared to Figure 5 we can see that it only takes a small change in incident angle to generate this behaviour because of the curvature of the band surface. We can observe this most clearly by comparing the slowness contours in Figures 5(a) and 6(a). In this setting the direction of the phase fronts also coincides with the

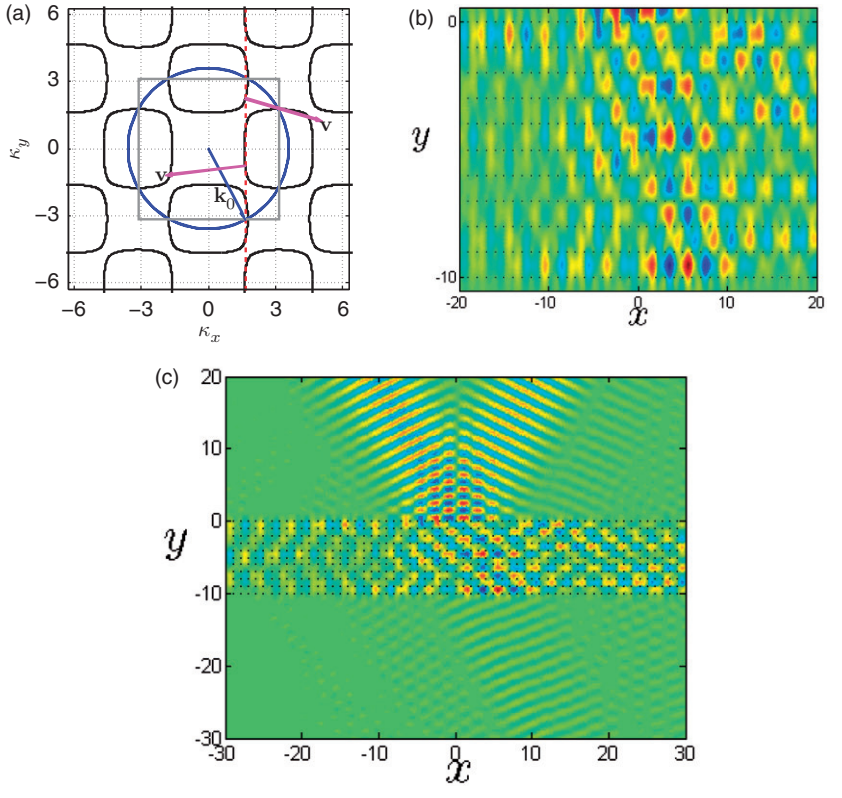

Figure 10. (Color online) (a): Slowness contour, and (b), (c): displacement (Re(u)) of the plate (where $k = 3.6022$, $k_{0x} = 1.65$, $\theta_i = 27.26^\circ$) for multiple ray instances (near trapped waves).

direction of the group velocity. In Figure 7 we give surface plots of the plate displacement when Rayleigh anomalies are encountered. Since Rayleigh anomalies are not a PlaC effect, but purely a grating effect, the slowness contours are not given, but generally speaking, Rayleigh anomalies are characterized by a 'passing off' effect where additional orders are excited ($\chi_{\pm p}$ for $p \neq 0$ switches from a purely imaginary number to a small, real value) giving rise to a secondary output beam which appears almost parallel to the grating [47–52]. The location of these anomalies can be determined analytically by specifying $\theta_i = \pm \pi/2$ in (39) and solving appropriately.

In Figure 7(a) we can clearly see this surface wave travelling in the direction of $x \to -\infty$ both above and below the crystal. Above the PlaC we can see a small trough of minimal displacement caused by the interaction of the Rayleigh anomaly wave with the incident Gaussian beam. For this particular example we have $\chi_{-1} = 0.0662$, $\chi_0 = 2.3180$ and $\mathrm{Im}(\chi_p) > 8$ for all other p demonstrating that only a very small angular change is required to observe this effect.

We show one further example of the different scattering behaviour exhibited by PlaCs for similarly shallow θ_c values in Figure 8. Here we see the formation of clearly defined peaks inside the crystal, which appear to be formed by the Gaussian beam reflecting off the far wall of the PlaC. These antisymmetric peaks are strongest in even numbered channels, and clearly outline the zero displacement condition along

each row of pins. Above the crystal we see a shallow reflected wave forming a clear channel of minimal displacement. This particular configuration corresponds to a high effective index (and $|p|$ value), which is typically associated with high reflection in photonics.

The final two examples in Figures 9 and 10 correspond to where standard ray tracing methods fail completely, as a unique physical cut for the group velocity vector in the slowness contours cannot be obtained. In particular, Figure 9 has an infinite number of directions supported where the k_{0x} line intersects the band surface contours, and Figure 10(a) yields multiple directions (two rays are possible here). In both cases the behaviour inside the crystal is associated with near trapped waves where our matrix of Green's functions has complex roots with $|\mathrm{Im}(k)| \simeq 0$. These two examples here sit in the neighbourhood of the interwoven arcs of high and low $|p|$, where a similar behaviour is observed throughout. These highly leaky waveguide modes can propagate some distance inside the crystal, but nevertheless cause a complicated pattern inside, as seen in Figures 9(b), 9(c), 10(b) and 10(c).

8. Summary

In this paper we have demonstrated how to construct the solution to the problem of Gaussian beam incidence on a PlaC. From the homogeneous problem of a doubly periodic infinite array of pins we were able to construct the first band surface for a square array, which was then used to determine the primary wave direction inside the PlaC. In addition to this we have computed the resolution parameters p, q, r and the effective index for our doubly periodic array to determine the input angle sensitivity and speed of the waves inside. We have given a brief survey of the diverse wave phenomena across the first Brillouin zone revealing how this simple platonic system exhibits many of the complex behaviours observed in photonic crystals. Here we do not observe any qualitative differences between the two crystal types, which is consistent with the fact that the biharmonic plate equation decomposes into Helmholtz (and modified Helmholtz) operators. However, quantitative differences could be expected for various other phenomena, since the presence of the modified Helmholtz operator can potentially strengthen the role of evanescent over propagating waves, leading to stronger trapped wave effects. Thus the photonic crystal literature can be used as a guide in the construction of novel devices for guiding and dispersing flexural waves in structured plates.

Acknowledgements

M.J.A.S. would like to thank Dr Ara Asatryan from the University of Technology Sydney for the many fruitful discussions on Gaussian beams. The authors would also like to thank the reviewers for their helpful and constructive comments which have strengthened the paper.

Note

1. For convenience we refer to these as isofrequency contours hereafter.

References

[1] Y.K. Konenkov, *A Rayleigh-type flexural wave*, Sov. Phys. Acoust. 6 (1960), pp. 122–123.

[2] A.N. Norris and C. Vemula, *Scattering of flexural waves on thin plates*, Sound Vibrat. 181 (1995), pp. 115–125.

[3] M. Farhat, S. Guenneau, S. Enoch, A.B. Movchan, and G.G. Petursson, *Focussing bending waves via negative refraction in perforated thin plates*, Appl. Phys. Lett. 96 (2010), 081909.

[4] M.J.A. Smith, M.H. Meylan, and R.C. McPhedran, *Scattering by cavities of arbitrary shape in an infinite plate and associated vibration problems*, J. Sound Vibrat. 330 (2011), pp. 4029–4046.

[5] D. Evans and R. Porter, *Penetration of flexural waves through a periodically constrained thin elastic plate in vacuo and floating on water*, J. Eng. Math. 58 (2007), pp. 317–337.

[6] A.B. Movchan, N.V. Movchan, and R.C. McPhedran, *Bloch–Floquet bending waves in perforated thin plates*, Proc. Royal Soc. A: Math. Phys. Eng. Sci. 463 (2007), pp. 2505–2518.

[7] N.V. Movchan, R.C. McPhedran, A.B. Movchan, and C.G. Poulton, *Wave scattering by platonic grating stacks*, Proc. Royal Soc. A: Math. Phys. Eng. Sci. 465 (2009), pp. 3383–3400.

[8] M.H. Meylan and R.C. McPhedran, *Fast and slow interaction of elastic waves with platonic clusters*, Proc. Royal Soc. A: Math. Phys. Eng. Sci. 467 (2011), pp. 3509–3529.

[9] S.G. Haslinger, N.V. Movchan, A.B. Movchan, and R.C. McPhedran, *Transmission, trapping and filtering of waves in periodically constrained elastic plates*, Proc. Royal Soc. A: Math. Phys. Eng. Sci. 468 (2012), pp. 76–93.

[10] T. Antonakakis and R.V. Craster, *High-frequency asymptotics for microstructured thin elastic plates and platonics*, Proc. Royal Soc. A: Math. Phys. Eng. Sci. 468 (2012), pp. 1408–1427.

[11] N. Stenger, M. Wilhelm, and M. Wegener, *Experiments on elastic cloaking in thin plates*, Phys. Rev. Lett. 108 (2012), 014301.

[12] R.C. McPhedran and A.B. Movchan, *Cloaking comes out of the shadows*, Physics 5 (2012), p. 2.

[13] C.G. Poulton, A.B. Movchan, N.V. Movchan, and R.C. McPhedran, *Analytic theory of defects in periodically structured elastic plates*, Proc. Royal Soc. A: Math. Phys. Eng. Sci. 468 (2012), pp. 1196–1216.

[14] M.J.A. Smith, R. Porter, and T.D. Williams, *The effect on bending waves by defects in pinned elastic plates* (2012), In press. DOI: 10.1016/j.jsv.2012.06.013.

[15] L.L. Foldy, *The multiple scattering of waves. I. General theory of isotropic scattering by randomly distributed scatterers*, Phys. Rev. 67 (1945), pp. 107–119.

[16] C.M. Linton and P.A. Martin, *Semi-infinite arrays of isotropic point scatterers. A unified approach*, SIAM J. Appl. Math. 64 (2004), pp. 1035–1056.

[17] A.A. Krokhin, P. Halevi, and J. Arriaga, *Long-wavelength limit (homogenization) for two-dimensional photonic crystals*, Phys. Rev. B 65 (2002), 115208.

[18] C.G. Poulton, A.B. Movchan, R.C. McPhedran, N.A. Nicorovici, and Y.A. Antipov, *Eigenvalue problems for doubly periodic elastic structures and phononic band gaps*, Proc. Royal Soc. A: Math. Phys. Eng. Sci. 456 (2000), pp. 2543–2559.

[19] J.D. Joannopoulos, *Photonic Crystals: Molding the Flow of Light*, Princeton University Press, Princeton, 2008.

[20] X. Hu, Y. Shen, X. Liu, R. Fu, and J. Zi, *Superlensing effect in liquid surface waves*, Phys. Rev. E 69 (2004), 030201.

[21] J.B. Pendry, *Negative refraction makes a perfect lens*, Phys. Rev. Lett. 85 (2000), pp. 3966–3969.

[22] X. Zhang and Z. Liu, *Negative refraction of acoustic waves in two-dimensional phononic crystals*, Appl. Phys. Lett. 85 (2004), pp. 341–343.
[23] C.G. Poulton, R.C. McPhedran, N.A. Nicorovici, and L.C. Botten, *Localized Greens functions for a two-dimensional periodic material*, in in *IUTAM Symposium on Asymptotics, Singularities and Homogenisation in Problems of Mechanics*, A.B. Movchan, ed., The University of Liverpool, Springer, 2004, pp. 181–190.
[24] A.B. Movchan, N.V. Movchan, and C.G. Poulton, *Asymptotic Models of Fields in Dilute and Densely Packed Composites*, Imperial College Press, London, 2002.
[25] S.K. Chin, N.A. Nicorovici, and R.C. McPhedran, *Green's function and lattice sums for electromagnetic scattering by a square array of cylinders*, Phys. Rev. E 49 (1994), pp. 4590–4602.
[26] V. Twersky, *Elementary function representations of Schlomilch series*, Arch. Rational Mechan. Anal. 8 (1961), pp. 323–332.
[27] T. Baba and M. Nakamura, *Photonic crystal light deflection devices using the superprism effect*, IEEE J. Quantum Electron. 38 (2002), pp. 909–914.
[28] H. Kosaka, T. Kawashima, A. Tomita, M. Notomi, T. Tamamura, T. Sato, and S. Kawakami, *Superprism phenomena in photonic crystals*, Phys. Rev. B 58 (1998), pp. 10096–10099.
[29] M.J. Steel, R. Zoli, C. Grillet, R.C. McPhedran, C.M. Sterkede, A. Norton, P. Bassi, and B.J. Eggleton, *Analytic properties of photonic crystal superprism parameters*, Phys. Rev. E 71 (2005), 056608.
[30] J.B. Pendry and D.R. Smith, *The quest for the superlens*, Scientific American 295 (2006), pp. 60–67.
[31] A.Z. Elsherbeni, M. Hamid, and G. Tian, *Iterative scattering of a Gaussian beam by an array of circular conducting and dielectric cylinders*, J. Electromag. Waves Appl. 7 (1993), pp. 1323–1342.
[32] G.D. Marshall, D.J. Kan, A.A. Asatryan, L.C. Botten, and M.J. Withford, *Transverse coupling to the core of a photonic crystal fiber: The photo-inscription of gratings*, Opt. Express 15 (2007), pp. 7876–7887.
[33] V. Cerveny and I. Psencik, *Gaussian beams and paraxial ray approximation in three dimensional elastic inhomogeneous media*, J. Geophys. 53 (1983), pp. 1–15.
[34] V. Cerveny, *Gaussian beam synthetic seismograms*, J. Geophys. 58 (1985), pp. 44–72.
[35] A.P. Kiselev, *Localized light waves: Paraxial and exact solutions of the wave equation (a review)*, Opt. Spectrosc. 102 (2007), pp. 603–622.
[36] A. Joseph and K. Porsezian, *Stability criterion for Gaussian pulse propagation through negative index materials*, Phys. Rev. A 81 (2010), 023805.
[37] R.W. Ziolkowski, *Pulsed and CW Gaussian beam interactions with double negative metamaterial slabs*, Opt. Express 11 (2003), pp. 662–681.
[38] E. Cubukcu, K. Aydin, E. Ozbay, S. Foteinopoulou, and C.M. Soukoulis, *Electromagnetic waves: Negative refraction by photonic crystals*, Nature 423 (2003), pp. 604–605.
[39] P.V. Parimi, W.T. Lu, P. Vodo, and S. Sridhar, *Photonic crystals: Imaging by flat lens using negative refraction*, Nature 426 (2003), pp. 404–404.
[40] M. Born and E. Wolf, *Principles of Optics: Electromagnetic Theory of Propagation and Diffraction of Light* , 2nd ed., Pergamon Press, New York, 1964.
[41] M.K. Savage, *Seismic anisotropy and mantle deformation: what have we learned from shear wave splitting*, Rev. Geophys. 37 (1999), pp. 65–106.
[42] S.P. Timoshenko, *History of Strength of Materials: With a Brief Account of the History of the Theory of Elasticity and the Theory of Structures*, Dover, New York, 1983.
[43] E.T. Whittaker and G.N. Watson, *Modern Analysis*, Cambridge University Press, Cambridge, 1927.
[44] M. Abramowitz and I.A. Stegun, *Handbook of Mathematical Functions with Formulas, Graphs, and Mathematical Tables*, Dover, New York, 1972.

[45] T. Baba and T. Matsumoto, *Resolution of photonic crystal superprism*, Appl. Phys. Lett. 81 (2002), pp. 2325–2327.
[46] D. Maystre and S. Enoch, *Perfect lenses made with left-handed materials: Alices mirror?*, J. Opt. Soc. America A 21 (2004), pp. 122–131.
[47] J.E. Stewart and W.S. Gallaway, *Diffraction anomalies in grating spectrophotometers*, Appl. Opt. 1 (1962), pp. 421–429.
[48] U. Fano, *The theory of anomalous diffraction gratings and of quasi-stationary waves on metallic surfaces (Sommerfelds waves)*, J. Opt. Soc. America 31 (1941), pp. 213–222.
[49] B.S. Zhao, G. Meijer, and W. Schöllkopf, *Emerging beam resonances in atom diffraction from a reflection grating*, Phys. Rev. Lett. 104 (2010), 240404.
[50] R.C. McPhedran, *The diffraction of plane reflection gratings* [Phd thesis], University of Tasmania, Australia, 1973.
[51] R.C. McPhedran and M.D. Waterworth, *A theoretical demonstration of properties of grating anomalies (S-polarization)*, J. Mod. Opt. 19 (1972), pp. 877–892.
[52] R.C. McPhedran and M.D. Waterworth, *Properties of diffraction grating anomalies*, J. Mod. Opt. 20 (1973), pp. 533–547.

Appendix 1. Numerical evaluation

To evaluate the infinite integral in (11) we use Gauss–Hermite quadrature

$$\int_{-\infty}^{\infty} \mathrm{e}^{-x^2} f(x)\,\mathrm{d}x \simeq \sum_{l=1}^{M} w_l f(x_l), \tag{41a}$$

as outlined in (25.4.46) of [44], where x_l is the lth zero of the Hermite polynomial $H_M(x)$,

$$w_l = \frac{2^{M-1} M! \sqrt{\pi}}{M^2 [H_{M-1}(x_l)]^2}, \tag{41b}$$

are the associated weights, and M is the number of sampling points.

This allows us to numerically evaluate the finite integral representation as the following sum

$$w_G^i(x, y) = \sum_{l=1}^{M} f_l \, \mathrm{e}^{\mathrm{i}\beta_l x - \mathrm{i}\chi(\beta_l) y} \tag{42a}$$

where

$$f_l = \frac{w_l}{\sqrt{\pi}}, \quad \beta_l = \rho(2\alpha_l / W), \quad \text{and } \chi(\alpha) = \begin{cases} \sqrt{k^2 - \alpha^2}, & \text{if } |\alpha| \le k\ , \\ \mathrm{i}\sqrt{\alpha^2 - k^2} & \text{if } |\alpha| > k. \end{cases} \tag{42b}$$

To include the effect of the crystal we apply an identical technique to the evaluation of (12) and sum over all the plane wave fields to obtain

$$w_G(x, y) = \sum_{l=1}^{M} f_l \left\{ \mathrm{e}^{\mathrm{i}\beta_l x - \mathrm{i}\chi(\beta_l) y} + \sum_{n=1}^{N} a_n G(\mathbf{x}, \mathbf{x}_n) \right\}. \tag{43}$$

We observe that (42a) and (43) are both truncated Fourier series representations, and accordingly have a finite period which depends strongly on the sampling parameter M.

Given that our PlaC is finite, we can force the periodically repeating Gaussian beams out of our region of interest around the cluster by specifying a suitably large M. We find that $M \simeq 500$ works well, however we only compute the plane wave fields for $|f_l| > 10^{-7}$ and thus for most cases approximately 74 plane wave solutions are considered. This is of greater importance when considering Gaussian beam scattering by infinite grating layers as interactions between the beams may occur for complex scattering cases.